Investigating *Calotropis Procera* natural dye extracts and PEDOT:PSS hole transport material for dye-sensitized solar cells

A. Alami[1,2,*], A. Alachkar[3], S. Alasad[1], M. Alawadhi[4,5], D. Zhang[1,2],
H. Aljaghoub[6] and A. Elkeblawy[7]

[1]University of Sharjah, Department of Sustainable and Renewable Energy Engineering, 27272 Sharjah, United Arab Emirates
[2]University of Sharjah, Centre for Advanced Materials Research, 27272 Sharjah, United Arab Emirates
[3]American University of Sharjah, Department of Chemical Engineering, 26666 Sharjah, United Arab Emirates
[4]American University of Sharjah, Department of Mechanical Engineering, 26666 Sharjah, United Arab Emirates
[5]Dubai Police G.H.Q., Dubai, United Arab Emirates
[6]University of Sharjah, Department of Industrial Engineering and Engineering Management, 27272 Sharjah, United Arab Emirates
[7]University of Sharjah, Applied Biology Department, 27272 Sharjah, United Arab Emirates
[*]Correspondence: aalalami@sharjah.ac.ae

Abstract. In this work, natural dye extracts from *Calotropis Procera* are used as the main dye-sensitizer in solar cells. The *Calotropis* plant is a non-food item capable of surviving the harsh climate of the United Arab Emirates. Its incorporation into dye-sensitized solar cells is tested by constructing various cells, whose performance was also compared to that of more common chlorophyll-based dye extracts (i.e. spinach) as well as compared against a baseline cell sensitized with a synthetic ruthenium dye. The performance of the *Calotropis*-based cells was in general better than those with other natural sensitizers, but of course scored lower efficiency results when compared to cells built with synthetic dyes (0.075% compared to 5.11%). The advantage in using a natural sensitizer include facile extraction and preparation, low cost and abundance, since the *Calotropis* source has no competing applications in terms of food, livestock feed, etc. The figure-of-merit of cell output vs. cost for such cells makes them a good contender for further research and development effort to overcome the obvious drawbacks of stability and service longevity. Adding a hole-transport material to the cells in the form of PEDOT:PSS was also attempted to assess the enhancement it could provide to the cells. This did not yield the desired results and more experiments have to be done to better understand the interaction of each added layer to the original cell design.

Key words: *Calotropis Procera,* dye-sensitized solar cells, natural sensitizer, third generation photovoltaics.

INTRODUCTION

Solar energy, the energy emitted from the sun, is a promising renewable energy resource that is widely available, easily accessible, and non-exhaustible, in addition to that it is utilized in various applications (Kibria et al., 2014; Ushasree & Bora, 2019). Different materials and natural resources can be readily adapted for various eneryg applications, such in solar collectors (Palabinskis et al., 2008), electromagnetic shielding (Mironovs et al., 2014) or for anticorrosion coatings (Dastpak et al., 2020). Given these innumerable advantages, researchers are racing towards enhancing the efficiencies and economies of collecting and storing solar energy, specifically using solar cells. The creation of solar cells underwent several stages. Each stage, known as a generation, was developed to enhance the development process of solar cells (Alami et al., 2019). First generation solar cells, known as the conventional silicon-based solar cells, are the most widely used solar cells and account for almost 80% of all the developed solar cells in the world. Silicon-based solar cells have high efficiency and are durable; however, lately it surfaced that the market share of silicon-based solar cells is declining (Aghaei, 2012). This is due to the amount of energy required to develop solar cells which in return requires huge investments. Later on, second generation solar cells were developed utilizing thin film semiconductors, which led to a huge reduction in the required investments but also reduced the overall solar cell efficiency (Alami et al., 2019). To utilize the full potential of solar cells it is essential to find an optimal combination of the associated costs of solar cells and its relative efficiencies, this indicates that either a solution must be provided for better utilizing the silicon material or a replacement for the silicon material that optimizes the solar cells' efficiencies and significantly lowers its costs must be found. Consequently, third-generation solar cells were developed to acquire the silicon-based solar cells' high efficiencies and the costs of the thin film solar cells (Bharam & Day, 2012). This combination will allow for an efficient and cost-effective production of solar cells that will facilitate an easier process of fabricating the solar cells (Kibria et al., 2014). The current mainstream third-generation solar cell types are: organic/polymer based solar cells, perovskite based solar cells, and dye sensitized solar cells (DSSC) (Sharma et al., 2015). Fabricating organic based solar cells requires low amounts of energy in contrast to inorganic solar cells (Yuan et al., 2011). Organic based solar cells are mechanically flexible, lightweight (Ganesh et al., 2013), and have low processing and materials costs. However, the resulting efficiencies of the organic based solar cells have been found to be relatively low (Yuan et al., 2011). The advantages offered of developing organic based solar cells make them attractive for portable applications and other domestic usages (Ganesh et al., 2013). Another type of third-generation solar cells, perovskites based solar cells, have gained significant attention because of its relatively low costs (Zhou et al., 2018) and high efficiencies that can reach up to 25.5% (NREL, Best Research-Cell Efficiencies, (2021). https://www.nrel.gov), but it struggles to maintain these efficiencies as perovskites based solar cells tend to have issues in their stability and durability. A recent investigation have revealed that perovskites based solar cells will have an essential role in future electric automobiles batteries (Sharma et al., 2015). Dye Sensitized Solar Cells (DSSC), another type of third-generation solar cells, have reached efficiencies of about 13% and have had extensive attention from researchers and significant developments because of their relatively low costs, easy process, and high efficiencies (Zhou et al., 2018). Moreover,

their fabrication process can use several low cost organic materials and eliminates the incorporation of silicon within the process (Alami et al., 2019). A dye sensitizer, semiconductor electrode (p-type NiO, and n-type TiO$_2$), counter electrode, and the mesoporous media are the most essential parts of a DSSC. DSSCs utilize dye molecules in-between electrodes (Sharma et al., 2015). The most well-known type of DSSC is the n-type titanium dioxide (TiO$_2$) DSSC, where sunlight is absorbed by the surrounding molecular dye of the TiO$_2$. Once the sunlight penetrates the electrode passing through the molecular dye the electrons get excited and pass to the conduction band of the TiO$_2$. The electrode will collect the excited electrons as they pass through to power a load, afterwards the electrons re-enter the DSSC electrolyte on a counter electrode. The DSSC electrolyte brings the electrons to the dye molecules again (Tian et al., 2019). The photosynthesis process of the TiO$_2$ and the transparent dyes enhances the DSSC efficiency to higher than 10% (Sharma et al., 2015).

In this work we report on various designs of DSSC with a natural dye sensitizer extracted from Calotropis procera. The incorporation of the natural Calotropis in DSSCs is very attractive, since Calotropis is abundant in the Emirate of Sharjah and is known to be a non-food plant that grows wildly during all seasons. Baseline cells with ruthenium-based dyes and another chlorophyll-based dye (spinach) were also built to compare the efficiencies and power output with those having the natural dye. Besides the standard DSSC structure, we also investigated the effects of conductive polymer poly(3,4-ethylenedioxythiophene) polystyrene sulfonate (PEDOT:PSS) on both types of cells. The hole-transport material, PEDOT:PSS, was deposited on the counter electrode to examine if it would increase cell performance, with the possibility of replacing the conventional electrolyte setup. This would be an important advantage done since forgoing the electrolyte can enhance the service time of the cells and reduce its sensitivity to adverse operating conditions of heat and humidity that negatively affects electrolyte and cause evaporation and leakage. Our studies on the Calotropis natural sensitizer and DSSC designs with PEDOT:PSS polymer can provide insights into developing green, low cost and more stable solar cells.

MATERIALS AND METHODS

Experimental Setup
Preparation and deposition of TiO$_2$ on photoelectrode

The photoanode was bought from Techinstro, which consists of the fluorine-doped tin oxide (FTO) with dimensions of 25 mm × 25 mm × 2.2 mm and sheet resistivity ≤ 7 ohms/sq. The cleaning process was done in two phases and started with cleaning the glass sheets with ethanol and placing it in ultrasonic bath for 15 minutes, and with DI water for another 15 minutes, and then by rinsing it with DI water and ethanol, before which the glass sheets were dried. The sheets were kept for UV-ozone treatment for 15 minutes. After measuring the conductive side using a multimeter, the TiO$_2$ active side was restricted with an area of 0.25 cm^2 using a plastic tape on three sides of the glass sheet. 50 mg of TiO$_2$ with 10–25 nm nanoparticles size was grinded with 50 mg of polyethylene glycol using a mortar and pestle for 30 minutes to obtain a homogenous titanium oxide paste. The paste was then spread on a FTO glass sample using doctor blading method. Lastly, a heating process was done to solidify the paste in a furnace by

varying the temperature, starting at 325 °C, 375 °C, 450 °C, and finally to 500 °C (each temperature step took 20 minutes). The glass sheets were then allowed to cool to 60 °C, before being immersed in an Ru dye sensitizer and in natural dye solutions extracted from *Calotropis Procera* or spinach, storing it under dark for 24 hours for the dye adsorption. The cell structure and *Calotropis Procera* plant are shown in Fig. 1, a, b.
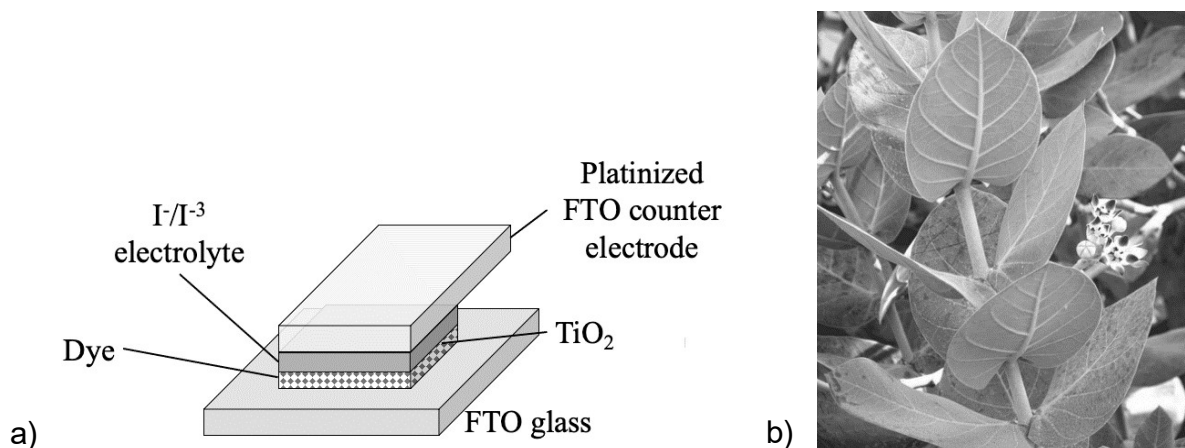
Figure 1. (a) Cell structure and (b) *Calotropis Procera* plant. Note that in (a) the PEDOT:PSS would be placed between the platinized electrode and the dye.

Dye extraction and FTIR analysis

For extracting and preparing natural dyes, leaves from *Calotropis Procera* or spinach were first washed with tap water and then rinsed with deionized water. For *Calotropis* dye extraction, the leaves were then cut into small pieces and kept to dry, the total mass is 36.3041 g which was immersed into a beaker before which the ethanol was added with a mass ratio of 3:1 of ethanol to leaves in balance, which resulted in 108.9123 g of ethanol. The beaker was then kept in an ultrasonic bath for one hour after covering it with parafilm. The spinach dye extraction for comparison with another natural sensitizer followed identical route. Lastly, a PTEF syringe with a porosity of 0.45 μm was used to filter the solution from any solid contaminants and the beaker was covered in a dark, cool environment to prevent dye oxidation.

Optical characterization

After putting the dye in cuvettes of transparent material (Ocean Optics Ultra Micro Cell with a range of 220–900 nm) and then on a cuvette holder, the optical absorbance of the solution was measured by a Maya 2,000 - Pro high-resolution spectrometers (Ocean Optics) with aHL - 2,000 tungsten halogen light source. Three Maya 2,000 spectrometers were used with software signal for measuring the UV-to-Infrared spectrum range (wavelength range from 200 nm to 1,100 nm @ 0.2 nm resolution). The same procedure was then replicated for spinach leaves to compare the dye pigments absorptivity.

As for dyes on TiO2, the optical assessments were also conducted using the same spectrometer. An ISP-REF integrating sphere with a WS-1 reflectance standard for calibration obtained from OceanOptics was used for the measurement of reflectance. The dyed titania electrodes transmissivity was estimated with an HL-2,000 tungsten halogen light source before it was converted into absorbance using the built-in software.

An integrating sphere (also from OceanOptics ISP-REF with an aperture of 0.4 inch, with a built-in tungsten halogen light source (Ocean Optics LS-1-LL) is used to measure specular and scattered reflectance. The baseline absorptance (0%) spectra were stored using the reflectance standard to assist comparison between the different compositions. To find the optical bandgap for each electrode, Tauc formula was then used.

A PerkinElmer spectrophotometer, USA in pressed-disc method using KBr pellets was used to record the Fourier Transform Infrared (FTIR) spectra. The FTIR range of operation was adjusted from 4,000 to 500 cm^{-1}, with 10 scans being signal-averaged having a resolution of 1.0 cm^{-1}.

Solar Cell manufacture

The solar cell was assembled by first joining the TiO_2 deposited electrode with platinum counter electrode (Solaronix.com) using binder clips. Injecting the drilled counter electrode with Iodolyte AN 50 electrolyte obtained from Solaronix (Solaronix.com) using a syringe. Next, for using the conductive PEDOT solution from Sigma Aldrich (sigmaaldrich.com) with or instead of the Iodolyte, the electrode was deposited with the PEDOT solution using a pipette and spin coating for 1 minute at 600 RPM. The electrode is then placed on a hotplate at 100 °C for 30 minutes and then allowed to cool down.

Cell characterization and impedance properties

Under an ABET SunLite solar simulator with AM1.5G and 100 mW cm^{-2} irradiance at a room temperature of 25 °C, the DSSCs current density-voltage (*J-V*) measurements were done using a Keithley 2400 SourceMeter.

Impedance analyzer potentiostat (VSP-300) under the sun simulator irradiation was used to obtain impedance spectra. 14.2 mV AC signal was supplied to the cell under 1-Sun conditions. The frequency range was changed between 100 kHz and 0.1 Hz with the bias voltage of the open circuit potential of the DSSC kept unchanged with a potential resolution of 20 μV. The Z-Fit analysis software from Bio-logic was used to fit the spectra. The tests are repeated three times for each cell and the average curve is reported and discussed.

RESULTS AND DISCUSSION

Dye FTIR analysis

For information on functional groups existent in the dye extract, FTIR is the appropriate tool. These peaks are often evidence for the existence of certain bonds and are shown in Fig. 2. All FTIR peaks present have been reported elsewhere (Ahliha et al., 2017). In the wave number range of 3,600–3,200 cm^{-1}, the O-H bond (polar group) manifests creating both intramolecular and intermolecular hydrogen bonds. Weak bonds at wave numbers 1,420–1,330 cm^{-1} were also observed due to the weakening of the in-plane O-H bending. Finally, infrared absorption shows at wave number 1,725–1,705 cm^{-1} causing the C=O stretching vibration. In general, the FTIR readings are all compatible with a green natural sensitizer with chlorophyl as a main pigment.

Dye optical properties

The Absorption tests of the dye solutions are shown in Fig. 3. It is noted that the *Calotropis* dye extract compares well with spinach, which is another dye based on the

chlorophyll pigment. It is noted, however that the absorptivity of the Calotropis dye is better in the visible range (~ 400–700 nm). This is expected result in better performance of the assembled DSSC as more photons are likely to enhance the photogeneration within the cell.
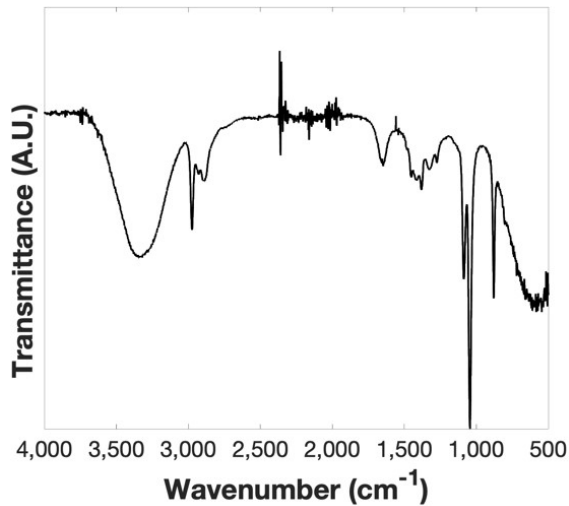
**Figure 2.** FTIR spectra of extracted *Calotropis Procera* dye.
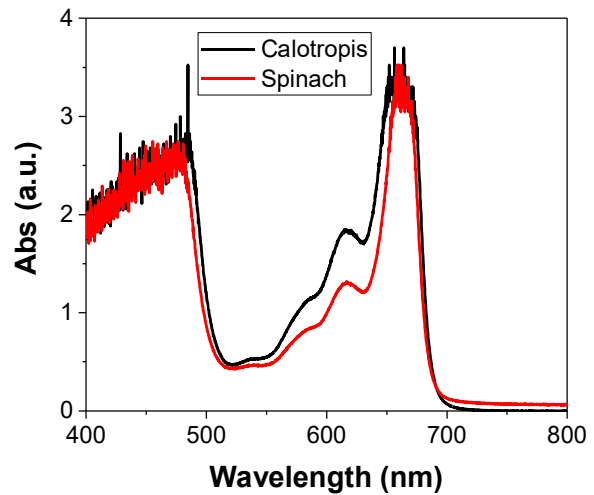
Figure 3. Absorption tests of *Calotropis* vs. spinach dye extracts

Absorptivity on TiO_2

Another optical assessment was done after extracting the dye from *Calotropis* leaves by adding the dye on a photoelectrode which consists of FTO with the deposited TiO_2 prior to cell assembly and testing. As shown in Fig. 4, the bandgap results are shown for one uncovered TiO_2 reference, an immersed electrode with a chlorophyll II pigment source (spinach) and also for the *Calotropis* dye. These results compare well with known natural sensitizer that is used in literature (Ahliha et al., 2017). The absorbance results are also shown inset.

For both spinach and *Calotropis* dyes at the violet-blue zone, the absorptivity graphs shown in Fig. 4 show a higher spectral absorption, with the former plateauing at the onset of the visible regime while the latter falls off towards the infrared. Considering that in Fig. 3 where *Calotropis* dye
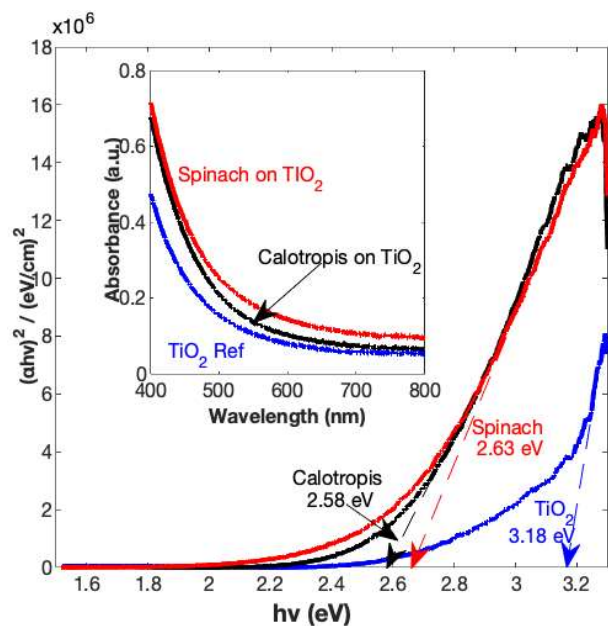
Figure 4. Bandgaps for prepared dye solutions loaded on TiO_2 material, calculated using Tauc formula for the *Calotropis Procera* dye, bare titania reference and another immersed in spinach. These values are calculated from absorbance values (inset).

solution shows higher absorptivity, the lower optical absorbance of *Calotropis* dye on photoelectrode compared to spinach is indicative of its insufficient adsorption onto the TiO_2 photoelectrode, which requires further improvement in the extraction method.

Cell testing results
Impedance testing

The impedance and frequency response results for the tested DSSC with *Calotropis* dye are shown in Fig. 5. The general shape of the obtained spectrum is the one normally obtained for DSSC at open circuit potential (Alami et al., 2019). A peak is found at the high frequency range, shown as an inset of Fig. 5, while a broad semicircle at the intermediate frequency range and lastly a tail at low frequencies. The behavior at high frequencies (inset) depicts the interface of the counter electrode and electrolyte. The charge transfer process occurs causing the shown perturbation in signal. Its small magnitude is an indication of the continued activity of the electrode and the potential of its enhancement for better performance of the cell. For intermediary frequencies, the peak is wide and is known to be due to electron diffusion in TiO_2 as well as the transfer of electron at the interface between TiO_2 and electrolyte. The electrolyte will degrade under illumination, causing its viscosity to change and hence hinder ion transport. This would be evident by the disappearance of this peak. Finally, a small tail appears at low frequencies which is known to correspond to the slow diffusion process of I_3^- in the electrolyte. For the present tests, the tri-iodide species concentration is low when compared to iodide ones which is advantageous in reducing losses due to recombination.

The Bode plot for the naturally sensitized cells is shown in Fig. 6, a. There are no wide scale peaks as a general linear trend is observed at low
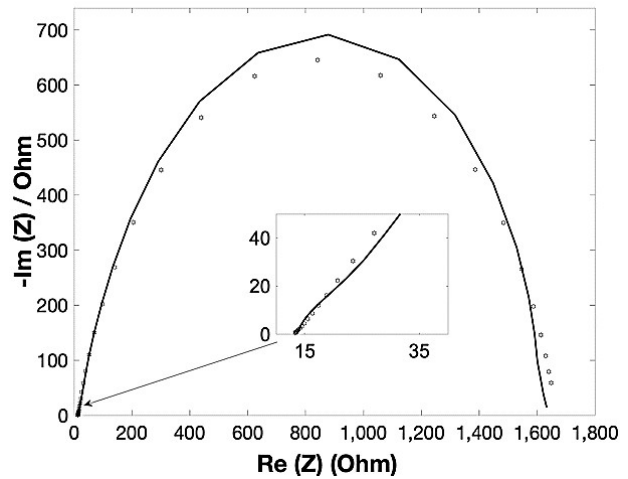
Figure 5. Impedance (Nyquist) test for the cell sensitized with *Calotropis* with the high frequency range results shown inset.
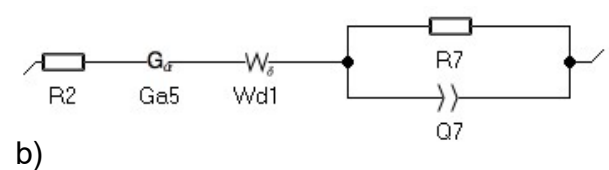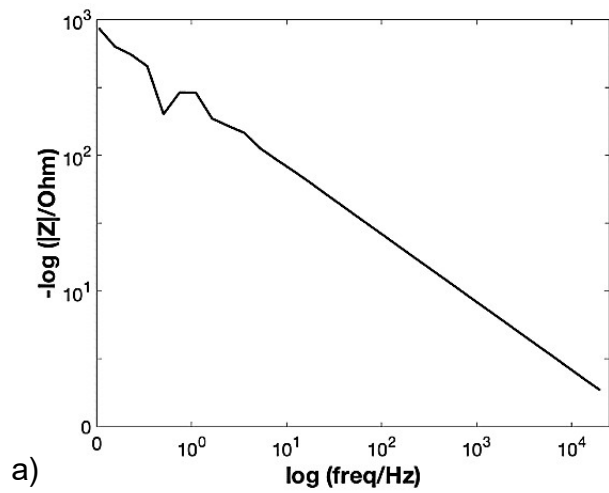

Figure 6. (a) The frequency response and (b) the proposed equivalent circuit for the cell sensitized with *Calotropis*.

frequencies. This indicates poor operational conditions of low rate of charge transfer at TiO_2/dye/electrolyte interface. This gives hope that better results can be obtained from the cell by applying better conditions of illumination, temperature or concentration. It is noted that the EIS data was fitted into the circuit model shown in Fig. 6, b. The components are as follows: R2 corresponding to the ohmic sheet resistance of the electrolyte, Ga5 resembling an electrochemical system with reflecting boundary where the distributed capacitance is replaced by distributed constant phase element (CPE) to account for non-ideality in the diffusion-recombination processes. The finite-length Warburg element (Wd1) was attributed to the transmission line model with short-. circuit terminus. Also, R7, Q7 are present at the counter electrode/electrolyte interface. It is important for a high functioning cell that the electron transport or diffusion resistance (R_d) be as small as possible and the electron recombination resistance be as large as possible and with a high diffusion coefficient, D

DSSC J-V characterizations

The standard structure DSSC (FTO / TiO_2:dye / I^-/I_3^- electrolyte / Pt / FTO) were assembled following the procedures detailed in the experimental section. The current density - voltage (J-V) characteristics of the various DSSCs are presented in Fig. 7 (Table 1 shows the summarized photovoltaic parameters).

a)

b)

c)
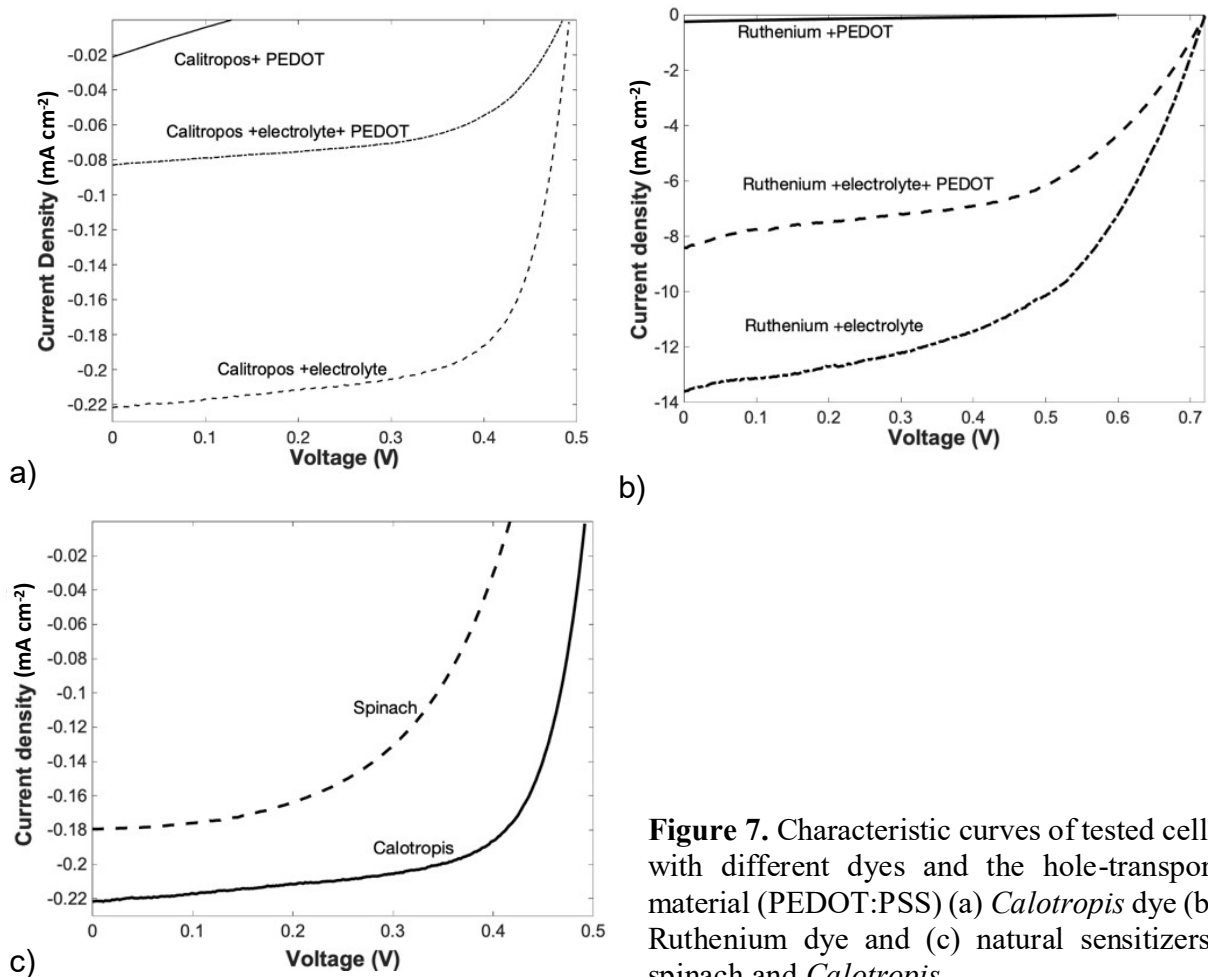
Figure 7. Characteristic curves of tested cells with different dyes and the hole-transport material (PEDOT:PSS) (a) *Calotropis* dye (b) Ruthenium dye and (c) natural sensitizers: spinach and *Calotropis*.

340

Comparing the standard cell structures in Fig. 7, a, the synthetic Ru-based sensitizer N719 showed good device performance in baseline DSSC, with a power conversion efficiency (PCE) of 5.1%. Differently, in the same device structure, the natural dyes extracted from the leaves of *Calotropis* and spinach both exhibited much lower cell performance (0.075% PCE). While the *Calotropis* cells demonstrated a slightly higher fill factor (FF) (~ 68% vs. ~ 52% for Ru-based cells), they are mainly limited by the small photocurrent density (0.22 mA cm^{-2}), which is more than one order less than the N719 dye. As such, the priority in future optimization for *Calotropis* DSSCs is increasing the dye loading ratio on TiO$_2$ photoelectrode, while adopting more efficient dye extraction methods. The smaller open-circuit voltage of the *Calotropis* cells is indicative of a smaller bandgap of the sensitizer.

Table 1. Summary of cell performance sorted by dye

Cell	Dye	Electrolyte	FF	PCE (%)	J_{sc} ($\frac{mA}{cm^2}$)	V_{oc} (V)
1	Ru	Iodolyte	0.52	5.11	13.6	0.72
2	Calotropis	Iodolyte	0.68	0.075	0.22	0.49
3	Ru	PEDOT	0.23	0.033	0.24	0.60
4	Calotropis	PEDOT	0.24	0.0006	0.022	0.13
5	Ru	PEDOT+Idolyte	0.51	3.083	8.41	0.72
6	Calotropis	PEDOT+Idolyte	0.57	0.023	0.083	0.486
7	Spinach	Iodolyte	0.52	0.04	0.18	0.41

As a further improvement to cell design and functionalities, the p-type conductive polymer PEDOT:PSS has been proposed to be an alternative for the Pt catalyst counter electrode (Lee et al., 2012), Hong et al. (2008), or replacing the liquid electrolyte for a quasi-solid-state cell design (Biancardo et al., 2007). Such incorporation can benefit DSSCs by reducing production cost, and/or mitigating issues from using liquid electrolyte (such as evaporation and leakage) and extending the cell lifetime. As a test trial, we further investigate the effects of PEDOT:PSS on the natural dye cells, with and without the presence of I$^-$/I$_3^-$ electrolyte. The results are shown in Fig. 7, b, c. It can be seen for both *Calotropis* and Ru-based cells that the addition of PEDOT:PSS polymer did not produce a direct benefit for the performance, as the J-V curves for both cells are considerably reduced in short-circuit current density (J$_{SC}$) when using both I$^-$/I$_3^-$ electrolyte and PEDOT:PSS. Furthermore, attempts at using PEDOT:PSS to replace the I$^-$/I$_3^-$ electrolyte entirely contributed to the further decline of device performance, as shown by the black curves in Fig. 7, b, c. The observation of the preliminary studies here suggests the need for future work on modifying the PEDOT:PSS material and investigating the interplay between PEDOT:PSS and the DSSC structure. On the other hand, the main advantage of using natural sensitizer would be the figure-of-merit that compares the efficiency of the cell with its potential cost. The ruthenium-based dye, bought from solaronix.com and 1 g of the material cost CHF 137 ($150). The natural dye that is extracted from a non-food plant that is abundant even in the harsh summers of the Gulf region, with costs of less than ~$1.5 per gram to extract the dye (cut the leaves, use ethanol at 1 gram of dye to 3 liter of ethanol). With these numbers, the figure of merit for a naturally sensitized solar cell would be around (0.075/1.5 = 0.05)

compared to that of a Ru-sensitizer: (5.11/150 = 0.032). These numbers are the same order of magnitude but with a clear advantage towards the naturally sensitized ones.

CONCLUSIONS

This work presented the construction of a dye-sensitized solar cell with the use of a natural sensitizer from a local non-food plant. The *Calotropis Procera* is a plant abundant in the United Arab Emirates, and its adaptation to the harsh weather and strong solar radiation makes it worthy of investigation for solar cell development. The dye extracted from the plant mainly contains chlorophyll pigments, but when compared to another natural sensitizer (spinach) it scored around 46% enhancement in efficiency. The *Calotropis* plant cannot be consumed by livestock or humans due to its skin irritation qualities, and hence it has this advantage as well over green plants such as spinach. A baseline cell was also constructed using a ruthenium-based sensitizer (N719) to ensure that the DSSC built would score acceptable results and is constructed well. At 5.11% efficiency, the cells did perform as hoped. Another track was also followed by adding PEDOT:PSS, which is a conductive polymer in place and in conjunction with the liquid electrolyte for a potential quasi-solid DSSC. This development, however, did not yield acceptable results and in fact was detrimental to the current extracted from the cells as well as their efficiency. More work will have to be done to overcome the potential limitations of such cells, such as the compatibility of the cells structures and other conductive materials at the counter electrode. Better sealing options can also be devised to limit electrolyte leakage and evaporation and keep dye material from degrading in the process.

REFERENCES

Aghaei, M. 2012. *A Review on Comparison between Traditional Silicon Solar Cells and Thin-Film CdTe Solar Cells*. Proceedings National Graduate Conference 2012 (NatGrad2012), 1–5.

Ahliha, A.H., Nurosyid, F.,Supriyanto, A. & Kusumaningsih, T. 2017. The chemical bonds effect of anthocyanin and chlorophyll dyes on TiO2for dye-sensitized solar cell (DSSC). *Journal of Physics: Conference Series* **909**(1), 12013. https://doi.org/10.1088/1742-6596/909/1/012013

Alami, A.H., Aokal, K., Zhang, D., Taieb, A., Faraj, M., Alhammadi, A., … & Irimia-Vladu, M. 2019. Low-cost dye-sensitized solar cells with ball-milled tellurium-doped graphene as counter electrodes and a natural sensitizer dye. *International Journal of Energy Research* **43**(11), 5824–5833. https://doi.org/10.1002/er.4684

Bharam, V. & Day, D. 2012. *Advantages and challenges of silicon in the photovoltaic cells*. Final Term Paper, 1–16.

Biancardo, M., West, K. & Krebs, F.C. 2007. Quasi-solid-state dye-sensitized solar cells: Pt and PEDOT:PSS counter electrodes applied to gel electrolyte assemblies. *Journal of Photochemistry and Photobiology A: Chemistry* **187**(2), 395–401. https://doi.org/https://doi.org/10.1016/j.jphotochem.2006.11.008

Dastpak, A., Wilson, B.P. & Lundström, M. 2020. Investigation of the anticorrosion performance of lignin coatings after crosslinking with triethyl phosphate and their adhesion to a polyurethane topcoat. *Agronomy Research* **18**(S1), 762–770. https://doi.org/10.15159/AR.20.061

Ganesh, B., Supriya, Y.V. & Vaddeswaram, G. 2013. Recent advancements and techniques in manufacture of solar cells: organic solar cells. *International Journal of Electronics and Computer Science Engineering* **2**(2), 565–573.

Hong, W., Xu, Y., Lu, G., Li, C. & Shi, G. 2008. Transparent graphene/PEDOT–PSS composite films as counter electrodes of dye-sensitized solar cells. *Electrochemistry Communications* **10**(10), 1555–1558. https://doi.org/https://doi.org/10.1016/j.elecom.2008.08.007

Kibria, M.T., Ahammed, A., Sony, S.M., Hossain, F. & Islam, S.U. 2014. A Review: Comparative studies on different generation solar cells technology. In *Proc. of 5th International Conference on Environmental Aspects of Bangladesh*, pp. 51–53.

Lee, K.S., Lee, Y., Lee, J.Y., Ahn, J.-H. & Park, J.H. 2012. Flexible and Platinum-Free Dye-Sensitized Solar Cells with Conducting-Polymer-Coated Graphene Counter Electrodes. *ChemSusChem* **5**(2), 379–382. https://doi.org/https://doi.org/10.1002/cssc.201100430

Mironovs, V., Lisicins, M., Boiko, I., Koppel, T., Zemchenkovs, V., Lapkovskis, V. & Shishkin, A. 2014. Cellular structures from perforated metallic tape and its application for electromagnetic shielding solutions. *Agronomy Research* **12**(1), 279–284.

Palabinskis, J., Aboltins, A. & Lauva, A. 2008. The comparative material investigations of solar collector. *Agronomy Research* **6**(S), 255–261.

Sharma, S., Jain, K.K. & Sharma, A. 2015. Solar cells: in research and applications – a review. *Materials Sciences and Applications* **6**(12), 1145.

Tian, H., Gardner, J., Edvinsson, T., Pati, P.B., Cong, J., Xu, B., Abrahamsson, M., Cappel, U.B., & Barea, E.M. 2019. CHAPTER 3 Dye-sensitised Solar Cells. In *Solar Energy Capture Materials*, pp. 89–152. The Royal Society of Chemistry. https://doi.org/10.1039/9781788013512-00089

Ushasree, P.M. & Bora, B. 2019. CHAPTER 1 Silicon Solar Cells. In *Solar Energy Capture Materials,* pp. 1–55. The Royal Society of Chemistry. https://doi.org/10.1039/9781788013512-00001

Yuan, Y., Reece, T. J., Sharma, P., Poddar, S., Ducharme, S., Gruverman, A., … & Huang, J. 2011. Efficiency enhancement in organic solar cells with ferroelectric polymers. *Nature Materials* **10**(4), 296–302.

Zhou, D., Zhou, T., Tian, Y., Zhu, X. & Tu, Y. 2018. Perovskite-Based Solar Cells: Materials, Methods, and Future Perspectives. *Journal of Nanomaterials* **2018**, 8148072. https://doi.org/10.1155/2018/8148072